Model of bores interaction in the swash

José Barale, Laurent Lacaze, Dominique Astruc, Rafael Almar, Luis Pedro Almeida

Coastal Engineering 192 (2024) 104564

Contents lists available at ScienceDirect

Coastal Engineering

journal homepage: www.elsevier.com/locate/coastaleng

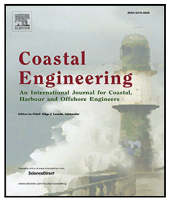

Model of bores interaction in the swash

José Barale [a], Laurent Lacaze [a,*], Dominique Astruc [a], Rafael Almar [b], Luis Pedro Almeida [c]

[a] Institut de Mécanique des Fluides de Toulouse (IMFT), Université de Toulouse, CNRS, Toulouse, France
[b] LEGOS (CNRS-IRD-CNES-University of Toulouse), Toulouse, France
[c] +ATLANTIC, Edifício LACS Estrada da Malveira da Serra, Cascais, Portugal

ARTICLE INFO

Keywords:
Swash
Wave interaction
Wave runup
Laboratory experiments

ABSTRACT

This paper examines the impact of wave interactions in the inner-surf zone, including the swash, on shoreline excursion dynamics. Specifically, the study focuses on how the time lag between consecutive waves and the slope of the beachface affect shoreline dynamics. To investigate this, a laboratory experimental setup is developed to study the behaviour of two consecutive bore-type waves travelling over a fluid layer with constant depth, representing an idealized inner-surf zone, before impacting an inclined solid plane with slope β, representing the beachface. Bore waves are generated using two dam-break flow devices, with a controlled time lag Δt between them. This simplified physical model allows for the assessment of semi-theoretical predictive models based on shallow water approximation, resulting in ballistic-type models for shoreline motion. By combining these approaches, the study characterizes different flow regimes in the $(\Delta t, \beta)$ parameter space. It is observed that varying Δt at a fixed β distinguishes four interaction regimes, either wave–wave interaction in the inner-surf zone or wave-swash interaction in the swash, with possibilities of merging or collision depending on wave orientation. In particular, increasing Δt leads to either bore–bore merging in the inner-surf, bore-runup merging in the swash, bore-backwash collision in the swash or bore–bore collision in the inner-surf. Bore–bore merging and bore-runup merging enhance runup, peaking when Δt is such that merging occurs near the transition from the inner-surf to the swash. On the contrary, bore-backwash collision results in additional dissipation of the second bore's dynamics, leading to a reduced shoreline extension compared to that induced by the first bore. All processes within the swash, including the transition between bore-runup and bore-backwash regimes, as well as the enhancement and extra dissipation of the second bore's swash excursion, exhibit some level of dependence on β. Overall, the results from this physical model help characterize and explain local mechanisms triggered by wave interaction near the shoreline. Validating this model's relevance warrants specific attention through comparisons with field data. As an initial validation attempt, field data extracted from the literature are compared to the physical model, showing promising agreement.

1. Introduction

It is now beyond doubt that understanding and characterizing the dynamics of the swash zone, delimiting the ocean surf-zone and dry coastal areas, are crucial to predict morphodynamics of natural beaches, large runup during storm and potential overtopping and breaching of dunes (Brocchini and Baldock, 2008; da Silva et al., 2020). Unfortunately, the full characterization of the complete dynamics of the swash zone, coupling complex mechanisms such as waves interactions, turbulent boundary layer, fluid–particles interaction, thin films, ..., all affected by local slope β, is still an ambitious and probably unreachable task for both measurement deployments and theoretical developments.

Yet, simple ballistic-type models of bore collapse onto slopping beach have been shown to lead to a reasonable prediction of swash excursion in nature (see for instance Bergsma et al., 2019, and references therein). Even if such models stem from advanced theoretical solutions in the shallow water approximation (Shen and Meyer, 1963; Hibberd and Peregrine, 1979; Guard and Baldock, 2007, see for instance), they are actually strongly simplified to provide usefulness for complex natural incoming wave forcing. This usually requires to prescribe an adequate parameterization of the physical processes involved, such as local dissipation along the beach and/or initial condition of the incoming bore, in order to capture the relevant dynamics. Now, such approach needs to be complemented and strengthened to include physical mechanisms allowing to capture excursion variability of the swash (Stockdon et al., 2006; Hughes et al., 2018; Rutten et al., 2021). Waves interaction is one of this mechanism which shall explain observed runup extensions, leading to overtopping or specific events of

* Corresponding author.
E-mail address: laurent.lacaze@imft.fr (L. Lacaze).

https://doi.org/10.1016/j.coastaleng.2024.104564
Received 10 December 2022; Received in revised form 6 May 2024; Accepted 17 June 2024
Available online 18 June 2024

substantial sediment transport in the swash zone (Baldock et al., 2011; Alsina and Cáceres, 2011; Cáceres and Alsina, 2012; Astruc et al., 2012; Hughes et al., 2018; Streicher et al., 2019; Chen et al., 2023). One of the reason for these observations is that these wave interactions play a significant role on the relative runup vs. backwash dynamics of two (or more) consecutive waves (Erikson et al., 2005; Hughes and Moseley, 2007; Brocchini and Baldock, 2008; García-Medina et al., 2017).

These waves interactions in the swash zone or close to it in the inner surf zone, also referred to as the wave–wave or wave-swash interaction depending on the actual location of the interaction, can be dissociated in two specific situations. First, hydrodynamics of consecutive bores leading to large runup extension is usually associated with bore-runup merging in the swash, or possibly bore–bore merging just prior the swash. Bore–bore and bore-runup merging events require wave celerity to be different from one wave to the other, the follower travelling faster. Such process will be referred to as the bore catch-up regime. Waves of different amplitude or a superimposed long wave inducing a local variation of the water depth and of the underlying flow velocity (García-Medina et al., 2017) such as with infragravity waves (Tissier et al., 2015; Padilla and Alsina, 2017; Bertin et al., 2018; De Bakker et al., 2016) are situations highlighting such difference in wave celerity, and leading to merging processes. On the other hand, a bore impacting the previous wave during its backwash phase, i.e. a bore-backwash collision, usually behaves oppositely onto the runup extension. But, it also leads to a more complex shear flow over the water column. The complex resulting flow can induce extra-suspension of sediment that favours an important transport (Alsina and Cáceres, 2011; Cáceres and Alsina, 2012; Bergsma et al., 2019). Dissociating the different scenarios leading to bore–bore merging, bore-runup merging and bore-backwash collision is not necessary an easy task.

In order to characterize the scenarios leading to the different wave–wave interaction regimes, it is useful to focus on two consecutive controlled wave bores. A simple laboratory model such as bore induced by a dam-break flow is thus quite useful. This configuration has been extensively studied in the case of a single event as it highlights several features of single swash event observed in real situations, while its full characterization remains possible (Hibberd and Peregrine, 1979; Yeh et al., 1989; Zhang and Liu, 2008; Antuono and Hogg, 2009; Mory et al., 2011; Pedersen et al., 2013; Zhu and Dodd, 2015). To our knowledge, the extension of this configuration towards the description of waves interaction using two consecutive bores has only been considered once in the literature (Chen et al., 2016). Chen et al. (2016) investigate and detail the hydrodynamics during interaction between two successive bores on a given beach slope 1/10, differentiating capture process and wave-backwash interaction process depending on the bore energy and the time lag between the two bores. A somehow similar configuration has been reported by Lo et al. (2013) and Pujara et al. (2015) using a different forcing leading to the case of two consecutive solitary waves. For a given swash slope 1/12, Pujara et al. (2015) showed that the runup of the second wave can be significantly reduced for some specific values of the time lag, smaller than the swash period of the first wave, between two successive solitary waves. Merging interaction leading to an increase of the second wave runup was not observed in their case. In their situation, the interaction process was attributed to a breaker type feature controlled by the ratio between the beach slope and the wave steepness. This is therefore slightly different mechanism than bore–bore interaction in the swash.

However, a complete understanding of the mechanisms leading to the observed regimes remains elusive, even in these simplified laboratory models. In particular, describing them through simple predictive models still merits specific attention in this configuration. Such objectives warrant further investigation by exploring a broader range of parameters. The main parameters controlling the swash interaction process in this configuration are the beach slope β, the time lag between the two consecutive events Δt, and their energy ratio. Part of this parameter space has been covered at constant β by Pujara et al. (2015) and Chen et al. (2016). We complement these previous studies by focusing on the influence of β and systematically varying the time lag Δt for two equal waves, i.e. fixing the energy ratio. We leverage the covered parameter space to propose a semi-theoretical model of wave interaction and associated runup, aiming to be useful for describing in-situ observations.

The present paper is therefore devoted to an experimental investigation of two consecutive bore waves evolving into an idealized inner surf zone prior impacting a beachface, modelled here by an inclined and impermeable plane. The two consecutive bore waves are generated experimentally using a double dam breaks device in a rectangular cross-section channel. Such device allows to propose and to validate idealized analytical models of waves interaction, as bore–bore merging, bore-runup merging and bore-backwash merging, extending ballistic-type model of bore collapse mentioned previously. Accordingly, two specific parameters which control the main physical processes of the wave interaction will be discussed: (i) the time lag Δt between the two consecutive waves and (ii) the slope β of the inclined plane modelling the beach. The paper is organized as follows. In Section 2, the experimental device is presented. Then the relevance of such bore-induced device is discussed in Section 3, also highlighting the relevance of the analytical assumptions made to predict the wave dynamics. Then, the more elaborate dynamics of the second bore, according to the dynamics of the preceding one, is presented in Section 5. An extension of the single wave analytical model to the dynamics of the following second bore is proposed. According to these device validations and model assumptions, swash-by-swash dynamics is then presented in Section 6. First, the bore–bore capture and bore-backwash collision processes are characterized, and then experimental data are compared to predictive models following assumptions verified in Sections 3 and 5.

2. Experimental setp-up

Two successive bores are generated using finite volume dam breaks slumping onto a 4 m long, 20 cm wide and 50 cm high glass channel of rectangular cross section. The channel is divided into three regions by two sluice gates connected to pneumatic actuators. From left to right as sketched in Fig. 1, the two first regions are reservoirs of equal length $l_2 = l_1 = 14.5$ cm, referred in the following to as $\mathcal{R}_2$ and $\mathcal{R}_1$ standing for the left-hand side reservoir and right-hand reservoir, respectively. The third region, referred to as the shore region, is composed of a flat bottom on its left part, followed by an inclined plane making an angle β with the horizontal on the right side of the tank. The two reservoirs are filled with water up to a equal height $h_1 = h_2$, while the shore region is filled up to a height $h_0 < h_1$. Coordinates x, y and z are aligned with the horizontal streamwise direction, spanwise direction and vertical direction respectively. The origin O of this coordinate frame is set at the frontier between $\mathcal{R}_1$ and the shore region (see Fig. 1). A coordinate frame is also attached to the inclined plane, denoted as X aligned along the inclined plane and Z is perpendicular to it. The origin for this second coordinate frame O_{sh} is chosen to correspond to the shoreline position at rest, i.e. the point of intersection of the still water level in the shore region and the inclined plane (see Fig. 1). In the frame (x, y, z), the position of the shore line is denoted $x = x_{sh}$, while it is $X = 0$ in the other frame. Note that in the present set of experiments, the length l_0 from O to O_{sh} slightly varies, ~12%, between experiments with changing β due to experimental limitations, but does not influence the discussion along the paper. To finish with, this physical model is aimed at mimicking the inner surf zone including the swash. For sake of clarity, we will refer to as the inner-surf, the region from the reservoirs to the initial shoreline at rest, i.e. $0 < x < x_{sh}$, and the swash as the region affected by the motion of the shore line, i.e. $X > 0$.

At $t = 0$, the sluice gate separating $\mathcal{R}_1$ and the shore region is removed, generating a first dam break flow which rapidly turns into a first bore propagating in the shore region. At $t = \Delta t > 0$, the second sluice gate, between $\mathcal{R}_1$ and $\mathcal{R}_2$, is removed, leading to the second

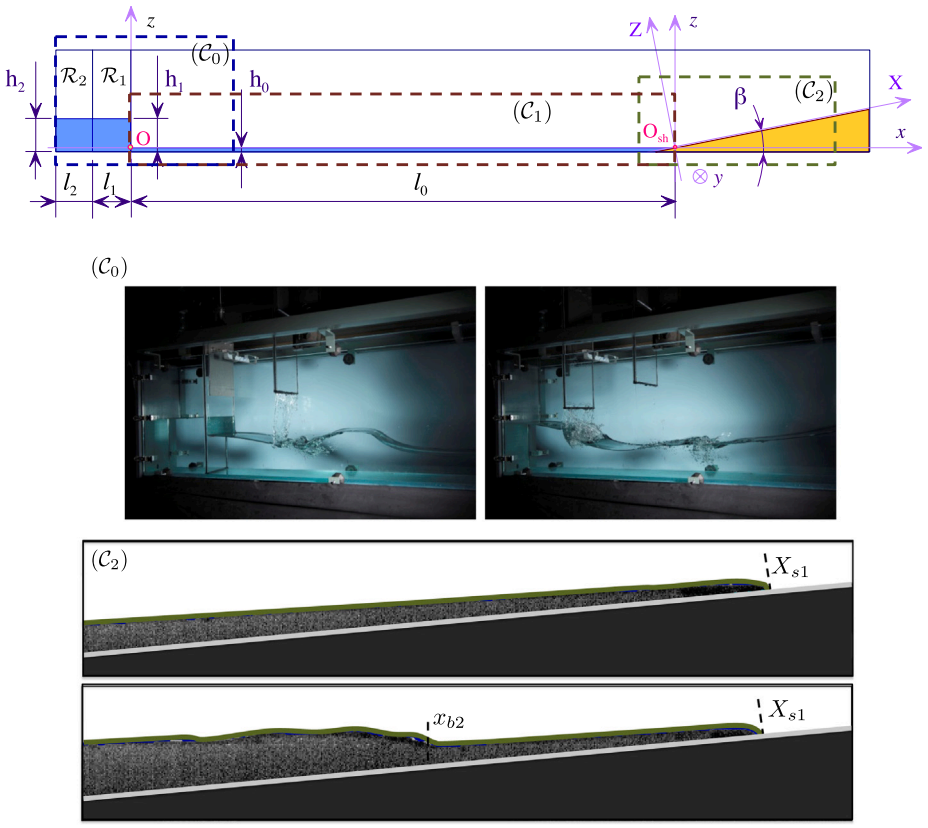

Fig. 1. From top to bottom. 2D Sketch of the experimental set-up (upper frame). Two snapshots of the initiation flow just after gate removals (camera C_0; middle row). Snapshots of one bore and two successive bores extracted from camera C_2 on the inclined plane (bottom row). Green lines correspond to the free-surface position extracted from image analysis, and grey line highlights the bottom inclined wall. The shoreline position induced by the swash of the first bore X_{s1} and the front position of the second bore x_{b2} as obtained in this study and discussed along the paper are also shown on view C_2.

propagating bore. Accordingly, $\Delta t \to \infty$ will refer to as a single bore configuration.

In the present study, three control parameters are varied, $h_1 = h_2 \in [3.1, 43.7]$ cm, $h_0 \in [2.2, 5.8]$ cm and $\Delta t \in [0.4, 2.1]$ s. The two former result in different dynamics of the generated waves. Accordingly, two geometrical dimensionless parameters can be constructed here, namely $\epsilon = h_1/h_0 - 1 \in [0.25, 8]$ and $\mu = h_0/l_1 \in [0.15, 0.4]$. These parameters control the type of generated wave. In the following, as we focus on bore propagation, μ is kept small, and ϵ is not too small, typically leading to breaking bore (Yeh et al., 1989). The last control parameter Δt provides different regimes of wave interaction as will be discussed along the paper. Finally, three different values of β are considered $\beta = 6°$, $\beta = 11°$, $\beta = 25°$, ranging from mainly dissipative towards strongly reflective regimes of the incoming waves interacting with the beach. Experimental parameters used along the paper are summarized in Table 1.

Qualitative visualizations of initial dam-break flows generating waves are obtained with a camera C_0 focusing on the left part of the channel (Fig. 1-C_0). The evolution of the wave flow along the channel is obtained using two 1280×1024 pixels high speed cameras (FASTCAM APX-RS @Photron), labelled C_1 and C_2, and a backlight source on the opposite side of the channel. Using a classical shadowgraphy method, the height profile $h(x,t)$ of the evolving free surface, and the associated water elevation $\eta(x,t)$ with respect to the initial rest state, are obtained in the (x,y) plane, allowing to quantify the wave characteristics (length and amplitude). More specifically, the first camera, C_1, images the region from $\mathcal{R}_1$ to O_{sh}, i.e. the region of bores propagation prior impact with the inclined plane. The length of the field in the x direction is ~3.1 m long, leading to a resolution of 2.4 mm/pix. The second camera, C_2, focuses on the region around the shore line rest position O_{sh} on a length scale about 80 cm along x, with a resolution 0.6 mm/pix. The acquisition rate is 300 Hz and the two cameras are synchronized and triggered by the pneumatic actuators control system. Typical snapshots and reconstruction of water level detection obtained using this device are shown in Fig. 1.

Table 1
Number of experimental runs and associated range of parameters (dimensional and dimensionless as defined in the text) used in the different sections of the paper. Note that $l_2 = l_1$, $h_2 = h_1$ and $l_0 \approx 340$ cm in Sections 5 and 6.

Section	Number of runs	h_0 (cm)	l_1 (cm)	h_1 (cm)	β (°)	Δt (s)
3	23	[2.2 : 5.8]	14.5	[3.1 : 43.7]	/	/
5	15	2.2	14.5	9.9	90	[0.4 : 2.1]
6	45	2.2	14.5	9.9	6, 11, 25	[0.4 : 2.1]

Section	$\epsilon \equiv h_1/h_0 - 1$	$\mu \equiv h_0/l_1$
3	[0.25 : 8]	[0.15 : 0.4]
5	3.5	0.15
6	3.5	0.15

In this paper, most of the discussion is based on the temporal evolution of the first and second bore positions in the inner-surf, x_{b1} and x_{b2} respectively, and their resulting shoreline motion in the swash, X_{s1} and X_{s2}. They are defined and obtained from the elevation height η extracted from the raw images. In particular, bore position is defined as the maximal value of $d(\eta)/dx$ upstream the wave, leading to the edge position of the bore x_b (see an illustration for the second bore position in image (C_2) of Fig. 1). Shoreline motion, X_s, is found as the intersection $\eta = (X_s(t), t) = \delta_\epsilon$ (see illustration of the swash induced by the first bore in image (C_2) of Fig. 1). Here δ_ϵ is a small constant value to threshold any remaining water film on the inclined plane. Its

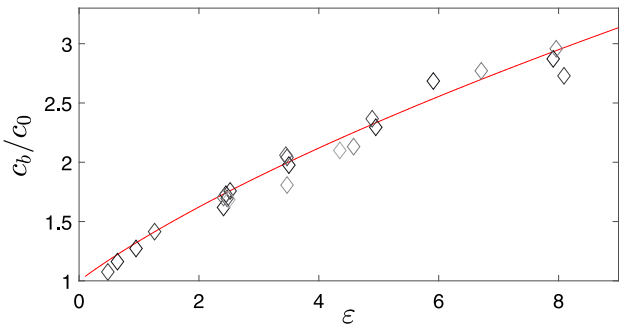

Fig. 2. Single bore evolution: bore celerity c_b as a function of ε. Symbols of various shades of grey correspond to different values of $\mu \in [0.15 : 0.4]$. Solid line corresponds to the shallow water solution (1).

specific value does not modify results as long as it is smaller that the bore height. It is chosen here as $\delta_\epsilon = 2$ mm, which is typically the order of the capillary length.

3. Preliminary investigation: the single wave model in the inner-surf zone

The knowledge of the dynamics of a single bore is first required as a base state for the description of interacting bores. We first investigate this situation, i.e. $\Delta t \to \infty$.. We propose here to characterize the dynamics of this bore from the initial state when evolving along the channel prior reaching the shoreline position O_{sh}.

In all cases considered here, the observed wave possesses the feature of a bore like wave with an abrupt change of free-surface height at the location of the front of the bore and a tail behind it which slowly decreases with x. This is associated with a roughly constant speed during its propagation prior reaching the inclined plane (zone covered by C_1 in the sketch of Fig. 1). Such bore mimics observed waves impacting the swash zone in many field observations.

The speed of the bore, denoted c_b, is obtained as the local velocity of the bore front, whose position $x_b(t)$ is extracted from height profile $h(x,t)$. After the initial slumping, and roughly along the first third of the flume, this velocity is found to be constant. This can be explained and predicted as follows. In the shallow water limit for an inviscid fluid, the hyperbolic system can be solved using the method of characteristics for a semi-infinite reservoir $\mathcal{R}$ as initial condition of the dam-break flow (Stoker, 1957; Stansby et al., 1998). Such solution requires to be connected to a bore-type singularity at the front of the slump, travelling from the reservoir towards the shore region on the layer of fluid h_0. Conservation of mass and momentum across the bore, leads to a constant velocity of the front c_b/c_0 with $c_0 = \sqrt{gh_0}$, which can be written as

$$F(c_b/c_0) - 2\,(1+\varepsilon)^{1/2} = 0, \tag{1}$$

with

$$F(\alpha) = \alpha - \frac{1}{4\alpha}\left(1+\sqrt{1+8\alpha^2}\right) + \sqrt{2}\left(\sqrt{1+8\alpha^2}-1\right)^{1/2}.$$

Note that the solution depends on ε, the non-linearity parameter, and not on μ, as this parameter is supposed asymptotically small in the shallow water approximation in accordance with the initial assumption of a semi-infinite reservoir.

The front velocities extracted from the experiments are compared with solution of Eq. (1) in Fig. 2, in which the dimensionless front velocity c_b/c_0 is plotted as a function of ε. We observe a good agreement despite the strong assumptions of the model compared with the experimental parameters considered here. Moreover, the symbols of various shades of grey in Fig. 2 correspond to different values of μ ranging in $[0.15 : 0.40]$, highlighting its weak influence on the dynamics of the generated bore in the range of parameter considered here. This confirms the shallowness of the considered flows in the present paper leading to bore wave type, according to field observation in the swash zone. This device is therefore relevant to mimic swash dynamics in that sense. We will see in the following that the length of the flume prior the inclined plane slightly affect the bore velocity. However, this is not a significant process, which can be simply accounted for, and thus it does not modify the discussion and conclusion drawn along the paper.

4. Regimes of waves interaction

A second bore wave is generated Δt s after the first one, with the same initial hydrodynamics conditions. In the following, the time lag between the two bores Δt and the beachface slope β are varied (see Table 1 for details). In this context, four different regimes of waves interactions are observed as illustrated in Fig. 3. They are obtained by varying Δt for all β, and delineated by three different critical lag-times denoted Δt_{sm}, Δt_{mc} and Δt_{sc}. The regimes correspond either to wave–wave interaction in the inner-surf zone, i.e. for $x < x_{sh}$, or to wave-swash interaction in the swash generated by the first bore, for $X > 0$. These different regimes are described in the following

At small enough Δt, the two consecutive bores merge prior impacting the beachface. This corresponds to a wave–wave interaction which will be referred to as a bore–bore merging. As it will be discussed in the next section, this regime is observed because the second bore can travel faster than the preceding one, even for two similar initial reservoir conditions. Then, increasing Δt above the critical value Δt_{sm} (swash-merging lower limit), this merging process stretches into the swash zone. The second bore merges here with the swash shoreline running up the inclined plane following the collapse of the first bore on the beachface, i.e. at $X > 0$. This regime corresponds to a wave-swash interaction and is referred to as the bore-runup merging. Beyond the second critical lag-time Δt_{mc} (merging-collision transition), the swash shoreline evolution induced by the first bore recedes thus initiating reflection prior interaction with the second bore. Then for $\Delta t > \Delta t_{mc}$, the second bore collides with the bachwash event, thus referred to as bore-backwash collision. Keeping increasing Δt, the swash event of the first bore is eventually completed and the first bore is fully reflected leading to a bore travelling backward prior collision. The resulting wave–wave interaction is thus referred to as the bore–bore collision and is obtained for $\Delta t > \Delta t_{sc}$ (swash-collision upper limit)

These regimes of interaction lead to very different dynamics, which are described and modelled in the following sections. In particular, bore–bore merging and the related Δt_{sm} do not depend on β, but on the length of the inner-surf l_0. As l_0 is kept constant in our experiments, Δt_{sm} is found constant $\Delta t_{sm} \approx 0.7$ s $= 14.8\sqrt{h_0/g}$. The dynamics leading to bore–bore merging is described in Section 5. On the other hand, wave-swash interactions, delineated by Δt_{mc} and Δt_{sc} are influenced by the beachface slope β. This will be studied in Section 6.

5. A wave catching up with a preceding one in the inner-surf zone

The bore–bore merging regime defined in Section 4 for $\Delta t < \Delta t_{sm}$, is obtained if the second bore can catch the first one in the inner-surf zone. To understand this mechanism, we focus here on the dynamics of the waves in the inner-surf zone. Accordingly, β is not a relevant parameter and is set to $\beta = 90°$ in this section (see Table 1 for details).

5.1. Experimental observations

In Fig. 4, the evolutions of front bore positions x_{b1} (solid blue lines) and x_{b2} (solid red lines) are plotted as a function of time t for different Δt. It can be first noted that the first bore x_{b1} is not affected by the presence of the following one, i.e. $x_{b1}(t)$ collapses on a single curve for all experiments performed with different Δt. Moreover, we observe that on a relatively long time scale, the first bore evolution slightly deviates

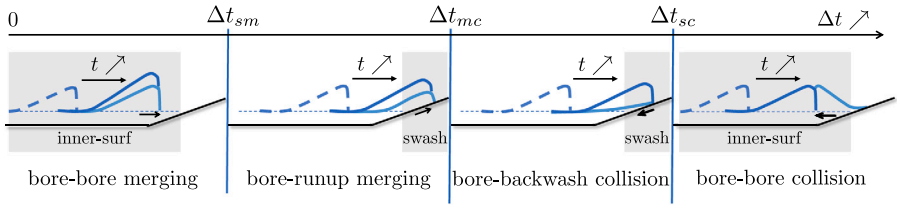

Fig. 3. Sketches of the different regime of waves interactions observed in the present study when increasing lag-time Δt between the two consecutive waves. Dark blue schematic elevations show the evolution of the second bore towards the beachface (from dashed line to solid line) and light blue elevation show the schematic shape associated with the first bore when interacting with the second one. Arrows indicate the direction of evolution for each wave with increasing time.

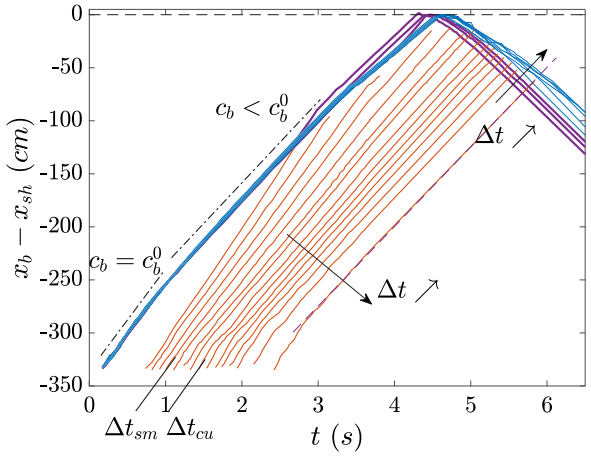

Fig. 4. Temporal evolution of several bore front positions $x_b(t)$ for different $\Delta t \in [0.4, 2.1]$ s: first bore $x_{b1}(t)$ (blue lines) and the following second bore $x_{b2}(t)$ (red lines). Each Δt corresponds to a couple of blue and red curves (blue lines are superimposed as the first bore dynamics is the same for different Δt prior interaction). Purple curves correspond to the trajectory of the remaining bore after waves interactions.

from the Stoker solution (1) discussed in the previous section (dash-dot line $c_b = c_b^0$, denoting c_b^0 the theoretical Stoker solution for the bore speed) towards a slower front evolution which can be estimated as being roughly constant on the considered time scale (dash-dot line $c_b < c_b^0$). This behaviour is actually observed for the two bores (dash line for the second bore at large Δt) and can therefore not be attributed to the bore interaction. Two main processes can affect this velocity. The first one is due to the finite volume of the initial reservoir, which differs from the supposed semi-infinite reservoir used to derived the theoretical solution. Accordingly, the possible role of a rarefaction wave on the evolution of the front, as often discussed in the literature of density-gravity currents (Rottman and Simpson, 1983; Hogg, 2006), shall be studied in future works. To the best of our knowledge such investigation has not yet been reported in the literature. The second process is associated with viscous dissipation at the bottom wall and side walls of the flume. Nevertheless, given the inertia of the generated flow in the inner-surf zone, this dissipation process is expected to be small compared to the finite volume contribution. Interestingly, even if the bore velocity during this phase is smaller than the Stoker solution c_b^0, we find that $c_b \approx \sqrt{g(h_0 + \eta_b^0)}$ with η_b^0 being the theoretical bore height obtained from Stoker solution.

On the other hand, Fig. 4 shows that the second bore can be significantly affected by the preceding one (red lines). In particular, given that the two bores are generated by the same initial reservoir condition, this figure demonstrates that the second bore can evolve faster than the single bore solution when influenced by the preceding one. This acceleration of the second bore along the flume compared to the preceding one is referred to as catching-up process. Its intensity varies depending on Δt. In particular, at relatively small Δt the second bore eventually reaches the first one prior impacting the inclined plane. Such process can actually be also observed for more complex wave forcing (Tissier et al., 2015; Padilla and Alsina, 2017). On the other hand, increasing Δt reduces this intensity of this process, eventually leading to a second wave having the same dynamics as the first one (see dotted line in Fig. 4).

According to the previous observation, a new critical time lag Δt_{cu} is defined, satisfying $\Delta t_{cu} > \Delta t_{sm}$. It allows to delineate the catching-up process when $\Delta t < \Delta t_{cu}$, from the other regime for which the two waves evolve similarly along the flume, for $\Delta t > \Delta t_{cu}$. It is found here to be $\Delta t_{cu} \approx 1.4$ s $= 29.6\sqrt{h_0/g}$.

The different behaviours above and below Δt_{cu} can be discussed according to the elevation height profiles $\eta(x,t) = h(x,t) - h_0$. For instance, η is plotted as a function of time at different positions x for $\Delta t = 1.8$ s $> \Delta t_{cu}$ in Fig. 5(a) and for $\Delta t = 0.5$ s $< \Delta t_{cu}$ in Fig. 5(b). For $\Delta t > \Delta t_{cu}$, the two successive bores, $b1$ and $b2$, remain nearly similar along the flume, with a steep front bore followed by a smooth tail. On the other hand, for $\Delta t < \Delta t_{cu}$, a catching process is observed (Fig. 5(b)). In this case, the second front is seen to catch the first one on finite time (from black profile to light grey profile). It is also interesting to note, that the second bore climbs on the tail of the preceding one with a front elevation above the tail of the preceding one, which remains nearly the same as the single bore case (≈2 cm here).

5.2. Modelling the evolution of two consecutive bores prior impacting the beach

A generic approach is proposed to predict the entire dynamics of the two consecutive bores, based on the observation reported in the previous section and including the mechanisms of the catch-up process described and characterized in detail in Appendix A. For sake of conciseness, we develop the model for two identical initial water columns in reservoirs $\mathcal{R}_1$ and $\mathcal{R}_2$, i.e. $l_1 = l_2 \equiv l$ and $h_1 = h_2 \equiv h$.

A typical sketch of the model is shown in Fig. 6. The bore evolving in the channel is assumed to roughly follow a triangular shape, in term of water surface deformation, as observed in experiments (see Fig. 5 for instance). The bore reaches such mature shape when the entire volume in the reservoir has been evacuated, say at $t = t_b$ and $t = \Delta t + t_b$ for the first bore and second bore respectively (see Fig. 6). These time scales are estimated as $t_b = (L - l)/c_b$ with $L = 2(h - h_0)l/\eta_b$ the length of the bore. They are obtained assuming that the entire initial volume of the column transfers to the bore wave, and before the triangular bore fully forms, the initial slumping follows Stoker's solution. Moreover, The bore elevation at the edge of the wave, η_b, is assumed to be conserved along the channel until reaching the inclined plane and to be imposed by the Stoker's solution, i.e.

$$h_b \equiv \eta_b + h_0 = \frac{h_0}{2}\left(\sqrt{1 + \frac{8c_b^2}{gh_0}} - 1\right), \tag{2}$$

with c_b obtained from (1).

For $t > t_b$ (respectively $t > \Delta t + t_b$), one assumes that the first wave bore (respectively second wave bore) evolves without being deformed, particularly keeping their initial front elevation η_b, dictated

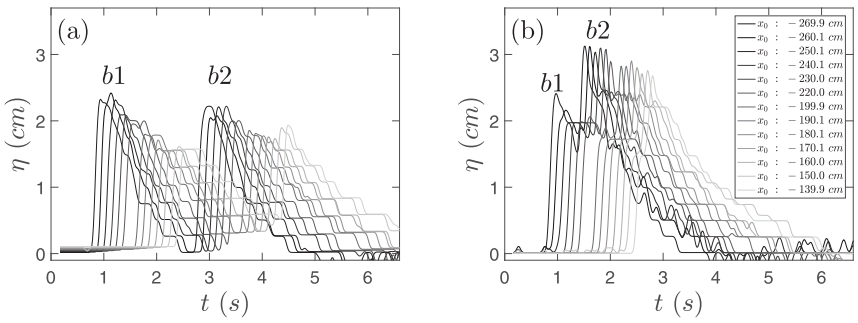

Fig. 5. Wave elevation η as a function of time t. Grey scales correspond to different streamwise location $x \in [-270, -140]$. (a) $\Delta t = 1.8$ s $> \Delta t_{cu}$; (b) $\Delta t = 0.5$ s $< \Delta t_{cu}$. $b1$ and $b2$ indicate water elevation associated with the first bore and second bore respectively. $x_0 = x_g - x_{sh}$ being the gauge position for each elevation signal shown here.

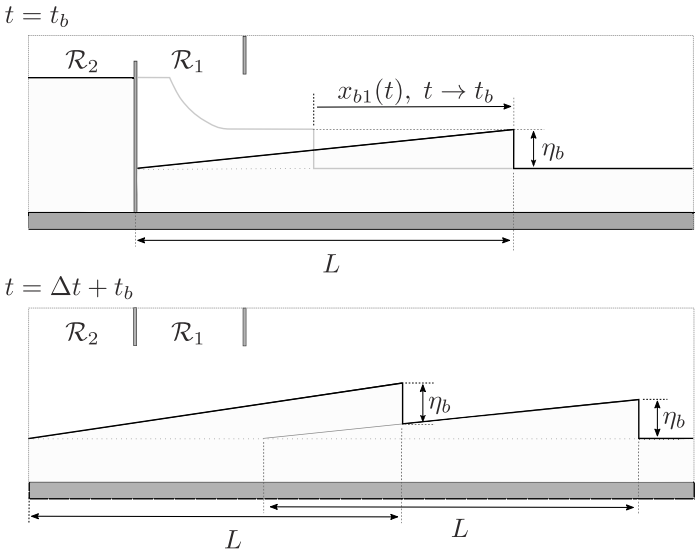

Fig. 6. Sketch of the model described in Section 5.2, corresponding to two bores generated by the same volume of fluid ($h_1 = h_2 \equiv h$; $l_1 = l_2 \equiv l$) in $\mathcal{R}_1$ and $\mathcal{R}_2$. At $t = t_b$ the evolving front x_{b1}, following Stoker's solution of an initial column collapse over a constant fluid layer depth h_0 (dotted line), has spread over a distance balancing the volume of $\mathcal{R}_1$ and a bore wave model of triangular shape of length L and front height η_b. This is referred to as the fully developed wave. At $t = \Delta t + t_b$ the second bore emanating from $\mathcal{R}_2$ is fully developed and evolves on the tail of the preceding one.

by the Stoker solution (2), and length L. Their velocity is constant and controlled by the maximum height at the bore front position, in the limit of long wave speed in the shallow water approximation. Note that these two assumptions, conservation of bores elevation and bore velocity, are based on experimental observation reported in Section 5.1. For the first wave, this leads to $c_{b1} = \sqrt{gh_b}$ for $t > t_b$. For the second wave, this can be slightly different, as the total height can vary when climbing on the tail of the first bore as discussed in the previous sections (see Fig. 6 for a sketch). The temporal evolution of the second bore front then depends on its position respectively to the first wave (see Fig. 6 for a sketch). In summary, we propose the following model for the evolution of the two fronts x_{b1} and x_{b2}, with respect to the shore line position

$$x_{b1}(t) = \begin{vmatrix} c_b t & \text{for} \quad t \le t_b \\ \sqrt{gh_b}(t - t_b) + (L - l) & \text{for} \quad t > t_b \end{vmatrix} \tag{3}$$

$$x_{b2}(t) = \begin{vmatrix} c_b(t - \Delta t) - l & & \text{for} \quad \Delta t < t \le \Delta t + t_b \\ \left.\begin{matrix} \sqrt{gh_b}(t - t_b - \Delta t) \\ +(L - 2l) \\ x_{b2}^{num} \end{matrix}\right| \begin{matrix} \\ \text{if} \quad \Delta t > (L - l)/\sqrt{gh_b} \\ \text{else} \end{matrix} & \left.\begin{matrix} \\ \\ \end{matrix}\right\} \text{for} \quad t > \Delta t + t_b, \end{vmatrix} \tag{4}$$

where x_{b2}^{num} is the numerical solution of

$$\frac{dx_{b2}}{dt} = \left(gh_b + g\frac{\eta_b}{L}(x_{b2} - \sqrt{gh_b}(t - t_b) + L) \right)^{1/2}.$$

The temporal evolution of the two wave fronts obtained from this model is reported in Fig. 7(b) for the same parameters as in the experiment discussed in Fig. 4 and reported here as Fig. 7(a) for clarity. Analytical model (3) for the first bore evolution is shown as blue line in Fig. 7(b). Numerical integration of x_{b2}^{num} from solution of (4) are reported as solid red lines for the range of Δt covered in the experiments. Note that an analytical equivalent of x_{b2}^{num} can be obtained in the limit $\eta_b \ll h_0$ (shown as dotted red lines in Fig. 7). Comparison with experimental data in 7(a) highlights the relevance of this simple model to capture the main features of the front dynamics of two consecutive bores at the surface of a constant depth water layer. In particular, the mains features of catch-up process discussed previously are actually recovered by this model. Note that this model is not designed to capture the merging of the bores when the second front has reached the first one, explaining why the second bore can overtake the first one in the model as seen in Fig. 7(b).

The results of the dynamics of two consecutive bores evolving over a fluid layer of constant depth, presented so far, show the ability of two consecutive bores to interact through a catch-up process. The whole

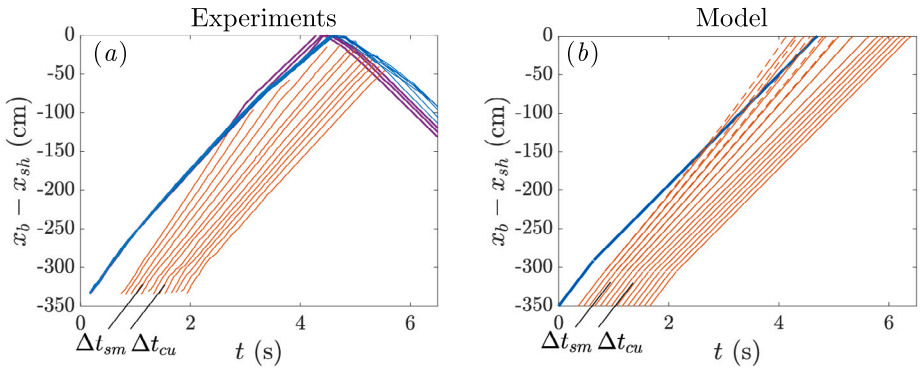

Fig. 7. Same as Fig. 4. Temporal evolution of all bore front positions extracted from the experiments (a) and from the model of Section 6.2 (b): first bore $x_{b1}(t)$ (blue line) and the following second bore $x_{b1}(t)$ (red lines). In (a), $\Delta t \in [0.4 : 0.1 : 1.6]$ s. In (b), $\Delta t \in [0.2 : 0.1 : 1.5]$ s.

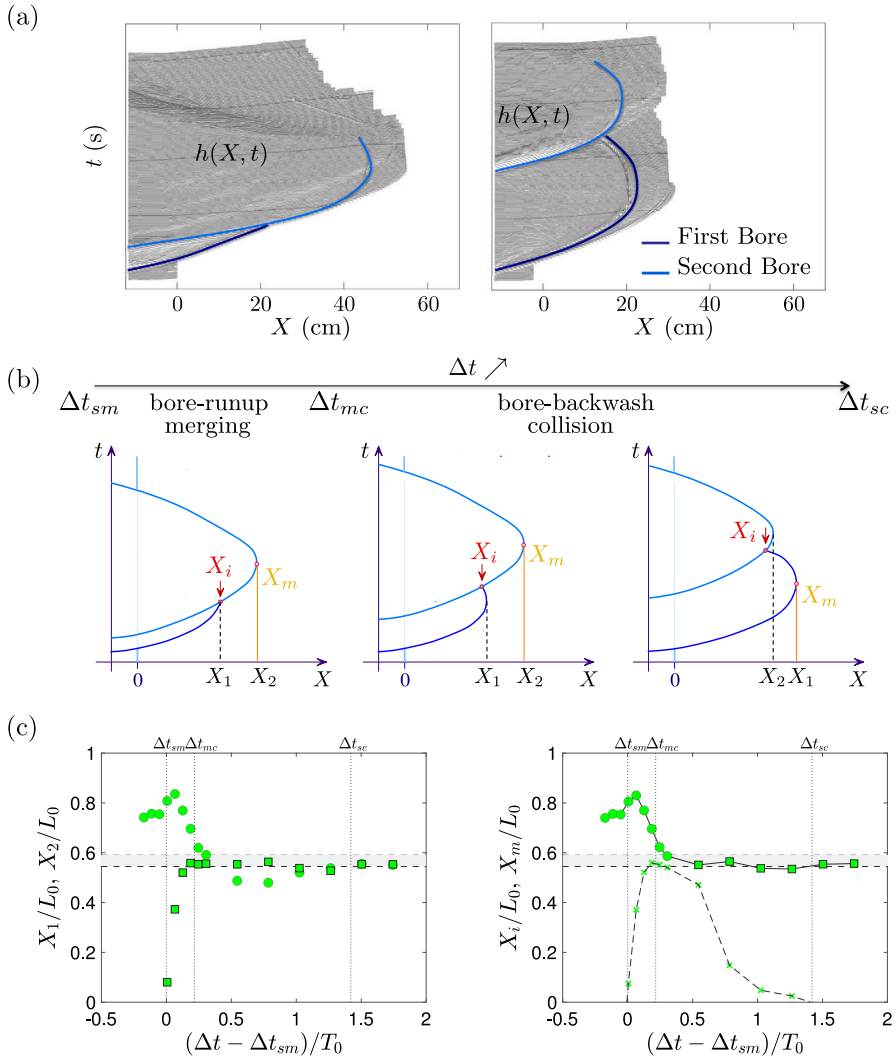

Fig. 8. (a) Examples of extracted shore line evolution. Grey lines highlight the spatiotemporal evolution of the water height h extracted from video in experiments, for a bore-runup merging (left) and a bore-backwash collision (right). Blue lines show the shoreline evolution induced by the first bore collapsing on the inclined plane X_{s1} (dark blue) and the second bore collapsing on the inclined plane X_{s2} (light blue). Note that non-zero height (grey lines) obtained beyond the bores position (solid blue lines) correspond to capillary-controlled water films which are removed from the analysis. Dark blue and light blue solid lines are both reported in (b) as sketches of the different types of shoreline evolution. (b) Sketch of the different types of interaction observed in the swash depending on Δt, with X_1 and X_2 the maximum spreading length of the first and second bore, respectively, $X_m = \max[X_1, X_2]$ the maximum spreading length of the whole swash event and X_i the localization of the interaction point between the two bores (see text for details). (c) dimensionless evolution of X_1 (squares) and X_2 (circles) -left plot- and X_m (squares and circles) and X_i (crosses) -right plot- as a function of Δt for $\beta = 6°$. L_0 and T_0 are defined in the text. Grey zone corresponds to the uncertainty range of the single bore extension.

dynamics of catch-up can be nicely prescribed by a simple geometric model. This can lead to the full merging of the two bores prior reaching the beach, i.e. the bore–bore merging for $\Delta t < \Delta t_{sm}$. In this case, a single resulting wave incomes the swash zone, with hydrodynamics properties

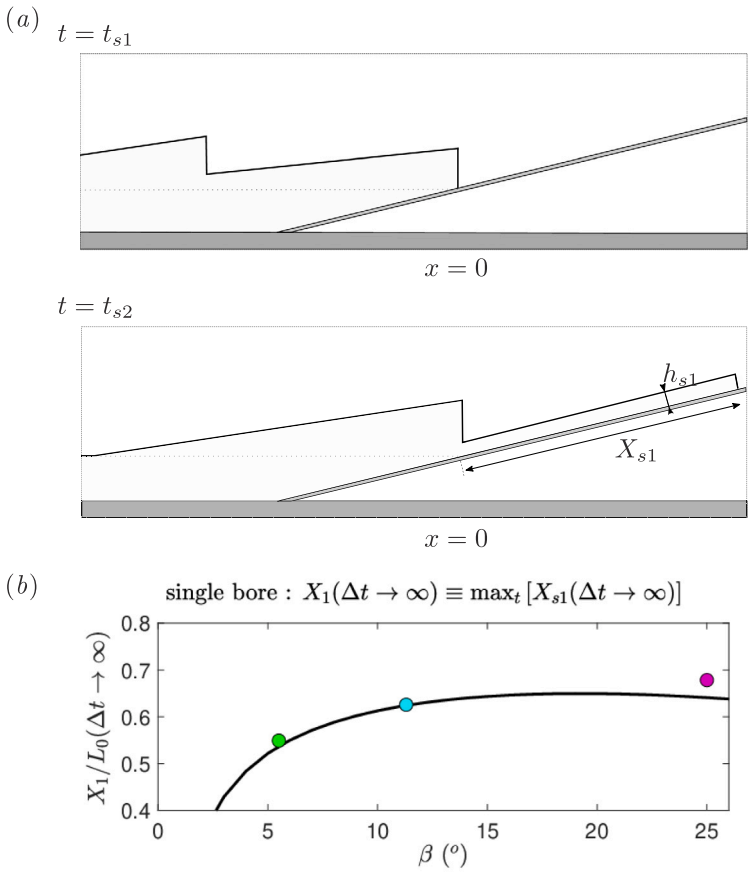

Fig. 9. (*a*) Sketch of the model described in Section 6.2, corresponding to two the two triangular bores modelled in Section 5.2 and sketched in Fig. 6, now impacting the inclined swash plane. At $t = t_{s1}$ the first bore reaches the shoreline $x = x_{sh}$, or equivalently $X = 0$ in the inclined frame. For $t > t_{s1}$, the first bore spreads over the inclined plane. This spreading is assumed to be characterized by a rectangular liquid film of constant height $h_{s1}(t)$ and length $X_{s1}(t)$. At $t = t_{s2}$ the second bore reaches $X = 0$. For $t > t_{s2}$, the spreading dynamics over the inclined plane is controlled by its initial condition at $t = t_{s2}$ depending on the characteristics of the first bore dynamics at this time, as detailed in the text. (*b*) Comparison of the single wave maximum spreading X_1 as a function of β between model (5) for $\nu_{eff} = 6\,10^{-4}$ m^2/s (solid line) and experiments (symbols).

resulting from this merging (not captured by the model as explained previously). On the other hand, the catch-up process can also lead to two waves incoming the swash zone, for $\Delta t_{sm} < \Delta t < \Delta t_{cu}$. In this case, initiation of catch-up prior the swash modifies the second bore dynamics with respect to the preceding one, mimicking the heterogeneity of wave dynamics in the inner-surf observed in more complex situations. These lead to various features on the swash dynamics. It will be shown in the following, how such mechanisms can modify the spreading length (run-up) of waves incoming the inclined beach.

6. Bores interaction in the swash zone

In this section, we describe the swash dynamics for $\beta = 6°$, $\beta = 11°$ and $\beta = 25°$ and the different values of $\Delta t \in [0.4 : 2.1]$ s (see Table 1), focusing to regimes $\Delta t_{sm} \leq \Delta t \leq \Delta t_{sc}$. In particular, the key objectives here are to highlight the influence of bore interactions and slope on the run-up – the maximum spreading of the shore line induced by the waves –.

6.1. General features and description

When catch-up process has fully developed prior the swash inclined plane, $\Delta t < \Delta t_{sm}$, a single bore enters the dry swash zone. This bore is a consequence of the merging between the two consecutive bores. On the other hand, when interaction occurs over the initially dry inclined plane, $\Delta t_{sm} < \Delta t < \Delta t_{sc}$, wave-swash interaction is obtained. In the latter case, two situations have been distinguished, bore-swash merging for $\Delta t < \Delta t_{mc}$ and bore-swash collision for $\Delta t_{mc} < \Delta t$ (see Section 4). This wide range of interaction processes leads to different features of the swash (see for instance Fig. 8(a–b)). Particularly, the spreading of the water mass over the inclined plane is strongly affected by the type of interaction, *merging* vs. *collision*, as will be discussed in the following.

Beyond the complex features reported here, simple interpretations and models are required, which could be extended for use in analysing field observations. Accordingly, we propose here to quantify the influence of the interaction on the swash extension, run-up, observed in the present configuration. For this purpose, the relation between run-up, Δt and β has to be established.

From the sketches of the different regimes observed in the swash zone (see Fig. 8(b)), four specific X-positions along the inclined plane can be defined to characterize the swash extension. Two of them are associated with the maximum spreading of each bore referred to as X_1 and X_2. We also define the maximum run-up X_m which can be either equal to X_1 or X_2 depending on the swash regime, i.e. on Δt. Finally, one defines the intersection position of the two consecutive bore X_i. Note that $X_i > 0$, i.e. inland compared to the initial shore line position, for $\Delta t_{sm} < \Delta t < \Delta t_{sc}$, i.e. for wave-swash interactions.

The evolution of these four swash lengths are plotted as a function of the time lag Δt in Fig. 8(c) for $\beta = 6°$, in a non-dimensional form. Here, we use $L_0 = \Delta h / \sin\beta$ and $T_0 = L_0/\sqrt{g h_0}$ as characteristic length

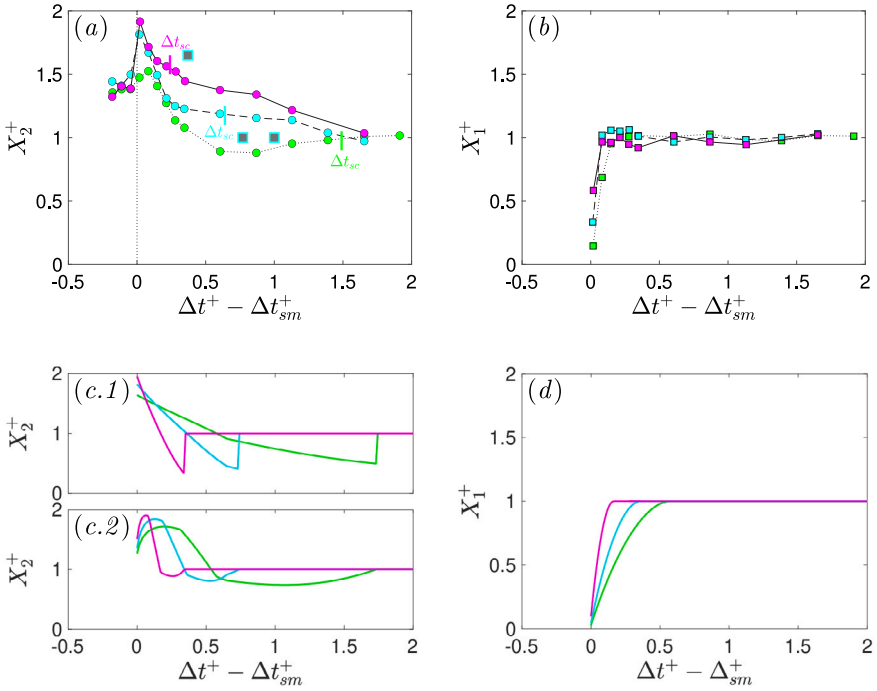

Fig. 10. Dimensionless Runup extension of the second bore X_2^+ (a,c) and first bore X_1^+ (b,d) as a function of the dimensionless time lag. (a,b) correspond to experiments and (c,d) correspond to model *A* (5)–(B.2) (c.1) and model *B* (5)–(B.3) (c.2). Green, cyan and magenta colours correspond to $\beta = 6°$, $\beta = 11°$ and $\beta = 25°$, respectively. In (a) square symbols correspond to data from field measurement extracted from Bergsma et al. (2019), where the upper beach slope is $\beta \approx 11°$.

and time scales, respectively. L_0 represents the projection of the initial column height along the inclined plane, indicating the potential spread of the swash if it could reach the same level of potential energy as in the initial reservoirs. T_0 denotes the time for the bore to extend to this length L_0 at the long wave speed $\sqrt{gh_0}$. In Fig. 8(c.left), we observe the first bore spreading X_1/L_0 (squares) and second bore spreading $X_2/L0$ (circles) as a function of $(\Delta t - \Delta t_{sm})/T_0$. Notably: (i) X_1/L_0 increases with $(\Delta t - \Delta t_{sm})/T_0$ from 0 to a maximum at $\Delta t = \Delta t_{mc}$ (bore-runup merging), corresponding to the single bore extension, and then remains constant for $\Delta t > \Delta t_{mc}$ (bore-backwash collision); and (ii) the second bore extension exhibits a non-trivial trend with Δt, showing a global maximum and a global minimum at finite Δt, eventually converging to the single bore extension at large Δt. These two observations can be understood as follows. (i) is due to the merging process, highlighted by increasing X_i/L_0 in Fig. 8(c.right). Once the swash enters the collision regime, $\Delta t > \Delta t_{mc}$, the spreading of the first bore remains constant regardless of Δt, indicating that it is no longer affected by the presence of the second bore. (ii) is influenced by the interaction between the first and second bores. The spreading of the second bore can be enhanced by the presence of the first bore, reaching a maximum for $\Delta t_{sm} < \Delta t < \Delta t_{mc}$. The maximum of X_2/L_0 obtained for $\Delta t \approx \Delta t_{sm}$ suggests a significant enhancement process when merging occurs at the swash. On the other hand, the second bore spreading can become smaller than the single bore spreading for bore-backwash collision (circles below dashed line for $\Delta t_{mc} < \Delta t < \Delta t_{sc}$). Here, backwash of the first bore prior collision, highlighted by decreasing X_i/L_0 in 8(c.right), induces extra-dissipation on the second bore dynamics leading to its smaller spreading in the swash. The resulting maximum run-up X_m/L_0 corresponding to either X_2 for $\Delta t < \Delta t_{mc}$ or X_1 for $\Delta t > \Delta t_{mc}$ is reported in Fig. 8(c.right).

The described swash extension characteristics, depending on Δt, were derived for a gentle slope of $\beta = 6°$, representing a dissipative slope, and correspond to the more comprehensive features observed in experiments. Similar patterns were observed for other slopes, including a maximum spreading of the second bore due to the merging process, although increasing β tends to lessen the impact of bore collision on reducing the extension of the second bore. These findings will be further explored later, as they do not significantly deviate from the discussed observations here. Before that, we introduce a simple predictive model in the next section, based on the aforementioned insights, aimed at capturing the various features observed in the case of small/dissipative slopes.

6.2. Modelling wave interaction in the swash

Following the approach developed in Section 5.2, we extend here the model to the swash dynamics, aiming at capturing the interaction processes obtained in the different regimes describe previously. For this purpose, one considers two consecutive swashes induced by the two consecutive bores, modelled in Section 5.2. Each swash is modelled using a ballistic model following the swash front. The interaction occurring between the two consecutive swashes is explained in the following and detailed in Appendix B

The main objective of the model is thus to provide the temporal evolution of the shoreline. Employing the geometric method outlined in Section 5.2, an overview of the swash geometry model is presented in Fig. 9(a). Specifically, we assume that the swash flow induced by each bore resembles a rectangular water layer characterized by $(X_s(t), h_s(t))$, representing its extension and thickness, respectively. These lengths fulfil a volume conservation condition assuming the swash volume matches that of the reservoir $\mathcal{R}$, i.e., $X_s(t) \times h_s(t) = (h - h0) \times l$. However, considering that the swash depth typically does not surpass the projected bore front η_b on the inclined plane, an additional cutoff condition $h_s(t) \leq \eta_b \cos\beta$ is imposed.

Then, the typical ballistic model used here to evaluate the shore line evolution X_s is written as

$$\frac{d^2X_s}{dt^2} = -g\sin\beta - \frac{C_D^{eff}}{h_s(t)}\left(\frac{dX_s}{dt}\right) \times \left|\frac{dX_s}{dt}\right|, \tag{5}$$

with $h_s(t)$ such as $h_{s1}(t) = \min[\eta_b \cos\beta, (h-h0)l/X_s(t)]$. The first term on the right hand side of (5) comes from the weight contribution along the slope, while the second term accounts for dissipation induced by inertial friction at the bottom, where C_D^{eff} denotes a drag coefficient requiring parameterization, as elaborated later on. Solving (5) necessitates an initial condition for the shoreline position and velocity. For both bores, we set the initial position as the shoreline at rest, $X = 0$, at t_{s1} and t_{s2} for the first and second bores, respectively. These times, derived from the inner-surf model outlined in Section 5.2, correspond to when the first and second bores reach the shoreline at rest. For the first bore, it can be explicitly written as $t_{s1} = t_b + (l_0 + l - L)/\sqrt{gh_b}$.

From now on, the approach to resolving the swash evolution for each bores differs. For the first bore, the initial velocity condition is $2\sqrt{g\eta_b \cos\beta}$, corresponding to the bore collapse velocity over an inclined plane β, often utilized in describing swash flows (Shen and Meyer, 1963; Yeh et al., 1989; Baldock and Holmes, 1999). It is worth noting that more intricate initial conditions have been proposed in the literature to offer more general solutions depending on incoming hydrodynamic forcing (Guard and Baldock, 2007). However, for the sake of simplicity and given the current state of our knowledge regarding the most suitable condition for achieving universality of solutions in a general scenario, we adhere to the simplest initial condition here. First, C_D^{eff} is calibrated using a single experiment to match the predicted maximum extension in this specific case. We employ the scenario where $\beta = 11°$ and $\Delta t \to \infty$, i.e., a single-wave situation, as the reference case. Consequently, we determine $C_D^{eff} = 2.510^{-2}$, which is fixed for the two bores thereafter. A comparison of the first bore maximum extension obtained using model (5) and experimental data is depicted as a function of β in Fig. 9(b). It is noteworthy that the first bore extension is always smaller than L_0, i.e. $X_1/L_0 < 1$, due to dissipation. This figure also illustrates the concept of dissipative vs. reflective beach, where the dissipation of the bore in the swash becomes increasingly significant as β decreases, resulting in a decrease in X_1/L_0 with decreasing β.

Modelling the swash induced by the dynamics of the second bore is considerably more intricate. It entails incorporating an interaction process into the ballistic model (5). Two models, denoted as model *A* and model *B*, are proposed to assess its dynamics. For clarity, these models are elaborated in detail in Appendix B. In both models, the depth of the preceding swash is disregarded when solving the evolution of the second event. Thus, the swash geometry mirrors that of the preceding bore (refer to Fig. 9(a)). In model *A*, only the initial velocity condition takes into account the presence of the first bore, while still solving (5) as the ballistic model, thus disregarding interaction over a finite period. The initial conditions are provided in Eqs. (B.2). In model *B*, interaction is considered over a finite period by modifying the friction term as long as $X_{s2} < X_{s1}$, i.e., when the second swash evolves over the first one. In this scenario, the friction term incorporates the difference in velocity between the two swash events. Additionally, the swash is assumed to be saturated during the run-up of the first bore, thus cancelling the influence of gravity on the dynamics of the second bore during this phase. The ballistic equations to be solved in this model then slightly differ from (5) and are presented in (B.3).

Results obtained with model *A* and model *B* will be discussed in the following section.

6.3. Influence of swash slope and waves lag

We now examine the influence of both Δt and β on the swash extension induced by the two bores, characterizing it through a comparison between experimental results and model predictions. Specifically, we investigate each bore extension relative to the single bore configuration obtained in the $\Delta t \to \infty$ limit, whose dependency on β has been previously discussed and presented in Fig. 9(b). Accordingly, we define the characteristic length scale as the maximal extension of the first bore $X_1(\beta, \Delta t \to \infty)$. The resulting dimensionless bore extensions are denoted as $X_1^+ = X_1/X_1(\beta, \Delta t \to \infty)$ and $X_2^+/X_1(\beta, \Delta t \to \infty)$, respectively. Here, X_1^+ tends towards 1 when Δt is large. Additionally, the characteristic time lag $T_{\Delta t}$ is chosen as the time required for one bore to travel its own wavelength over the constant fluid layer h_0, estimated from the wave model outlined in Section 5.2. Specifically, $T_{\Delta t} = L/c_b$ with $L = 2(h-h_0)l/\eta_b$ as proposed in Section 5.2 for the wavelength model, and with c_b and η_b obtained from (1) and (2), respectively. The associated dimensionless time lag is denoted as $\Delta t^+ = \Delta t/T_{\Delta t}$.[1]

Experimental results for the maximal extensions of the first bore, X_1^+, and the second bore, X_2^+, are presented for $\beta = 6°, 11°, 25°$ in Fig. 10(a–b) (green, cyan and magenta colours respectively). These extensions are plotted as a function $\Delta t^+ - \Delta t_m^+$, i.e. relative to the time lag at which the second bore reaches the first one at the shore line $X = 0$, according to the catch-up process. It can be summarize that (i) enhancement of the run-up induced by bore interaction, particularly through the *merging* process, is observed regardless of β, whether for dissipative or reflective swash slopes, (ii) maximal enhancement is consistently observed near the transition from bore-runup merging to bore-backwash collision, i.e. for $\Delta t^+ - \Delta t_{sm}^+ \gtrsim 0$, (iii) the run-up of the resulting second bore in the swash can be reduced due to *collision* process, particularly for small β, i.e. for dissipative swash; and (iv) the latter extra-dissipation process occurs for bore-backwash collision $\Delta t^+ < \Delta t_{sc}^+$.

These experimental results are compared with the models proposed in Section 6.2 (Fig. 10(c–d) for model *A* (c.1) and model *B* (c.2), (d) remains unchanged for both models). Recall that the only adjustable parameter here is $C_D eff$, obtained for a single bore experiment at $\beta = 11°$. Consequently, although the quantitative agreement between the models and the experiments is not perfect, it appears very reasonable as it largely captures the main features discussed so far. In particular, the qualitative trend for the second bore extension is captured, reflecting the primary features of enhancement and extra-dissipation mentioned previously. A maximal spreading of the second bore is obtained for all β at $\Delta t^+ = \Delta t_{sm}^+$. The extra-dissipation process of the second bore during bore-backwash collision, leading to a smaller extension of the second swash compared to the first one, $X_2^+ < 1$, is reproduced by the model (10(a)–(c)). However, in the model, this process is observed for all β, contrary to experimental results, where it is not observed at large β. In experiments at large β, an enhancement of the second bore is actually observed even during bore-backwash collision. In contrast, the mechanism captured by the models for bore-backwash collision suggests a reduction in the excursion of the second bore due to the negative acceleration induced by the first backwash, within the range of β covered here. This process even intensifies with increasing β for model *A*. In contrast, model *B* indicates a decrease in this process with increasing β, as suggested by the experiments. However, the models developed, in the state, are thus more suitable for moderate slope.

Finally, the global behaviours of the interaction between two consecutive bores on the swash extension can be analysed. Particularly, focusing on the slope β as a unique parameter, the time lag for *merging*-to-*collision* transition Δ_{mc}^+, the time lag for transition from bore-backwash collision to bore–bore collision Δ_{sc}^+, both relative to Δ_{sm}^+, and the maximal extension of the second bore at the transition from bore–bore merging to bore-runup merging $\max(X_2^+)$ are extracted. Their evolution as a function of β is reported in Fig. 11. Experimental data (symbols) are compared to the prediction of the model *A* (5)–(B.2) (black lines) and model *B* (5)–(B.3) (grey lines). The agreement is quite reasonable given the simplicity of the proposed models. The main trend, which characterizes the features of the interacting swash, is recovered, with a decrease in the characteristic time scales of swash

[1] Note that such time scale is different from T_0 used previously which was a relevant time for the dynamics of a single bore over an inclined plane but not for the time lag Δt.

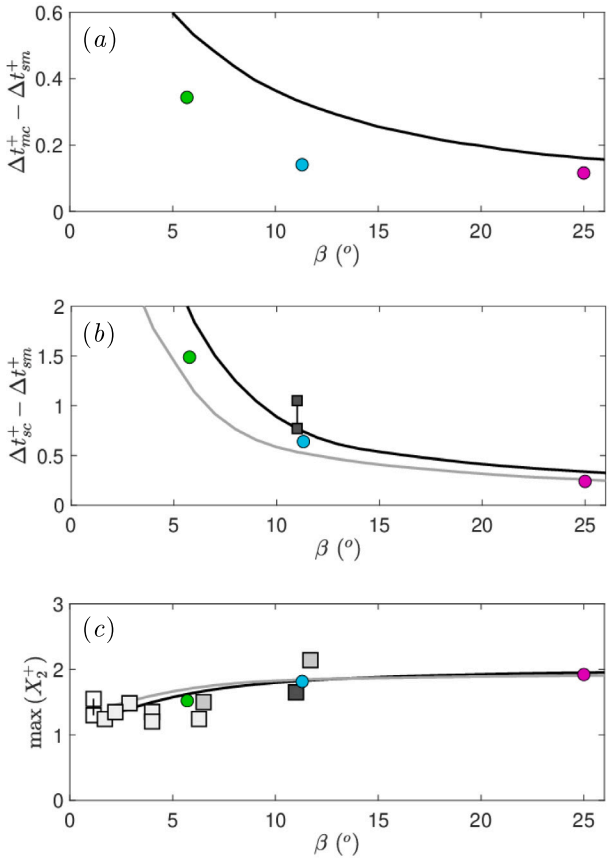

Fig. 11. Evolution of the characteristic features of the two-bore swash dynamics; experimental data (symbols), model *A* (5)–(B.2) (black solid lines) and model *B* (5)–(B.3) (grey solid lines) as a function of the beach slope angle β (°). (a) *merging*-to-*collision* transition Δt^+_{mc} and (b) transition from bore-backwash collision to bore–bore collision Δt^+_{sc}, both relatively to Δt^+_{sm}, i.e. the transition from bore–bore merging to bore-runup merging. (c) maximal second bore extension over time lag $\max(X_2^+)$. Some field data obtained from the literature are also shown here for comparison (square symbols from white-light grey to dark grey are extracted from García-Medina et al. (2017), Stringari and Power (2020), Alsina et al. (2018) and Bergsma et al. (2019), respectively. Note that from light grey to dark grey, more confidence is expected in extracting the quantities required for the purpose of the present paper as this was not the specific purpose of their studies.).

dynamics transitions with increasing β and an increase in the maximal run-up with β.

7. Discussion and conclusions

The aim of this study was to investigate bore interaction processes in the shoreline zone of coastal areas using an idealized laboratory model. Specifically, we focused on the interaction of two consecutive bores impacting a non-erodible inclined plane experimentally. In our laboratory model, an equivalent inner-surf zone was simulated by a fluid layer of constant depth over a flat bottom. Bores were generated by the dam break of two finite volume reservoirs, which were chosen to be equal in this case. Each generated bore then travelled over the surf zone before impacting an inclined swash plane. This approach allowed us to (i) identify the main influences of the time lag Δt between consecutive bores and the beachface slope β on the swash extension and (ii) propose geometrically-based models to capture the interaction processes of the two bores.

Two successive bores interacting in the inner-surf zone. Using this laboratory model, we described several steps of the wave interaction process sequentially. First, we modelled the dynamics of the first bore in the inner-surf zone using theoretical solutions in the shallow water approximation. This highlighted the relevance of such a modelling approach, which does not require parameter adjustment. Moreover, we showed that the dynamics of the second bore are influenced by the first bore, mostly controlled by the time lag Δt in the inner-surf zone. This interaction in the inner-surf zone was observed and modelled as a catch-up process, where the second bore evolves faster than the first one. Even with identical initial generation of the two bores, this process was attributed to the second bore climbing over the tail of the first one. The influence of the first bore was thus accounted for in a simple model, extending the previous single bore model to a situation of more complex background flow induced by the first one. An idealized geometrically-based model then allowed us to prescribe the dynamics of both bores in the inner-surf. It was demonstrated that such a simple model accurately predicts the dynamics of two consecutive bores.

Two successive bores interacting in the swash zone. The swash dynamics has been then investigated through the extraction and prediction of the shore line evolution, with a specific attention on the local maximum reached by the shoreline, as the runup length X_1 of the first bore and the runup length X_2 emerging from the second bore or as a consequence of the merging of the two bores prior reaching the inclined plane. Both the slope β and the time lag Δt have been shown to affect the dynamics of the swash. A common feature observed for all β is the enhancement of the second bore runup for a given range of Δt associated with the merging of the two bores, which is maximal when merging occurs close to the initial shore line at rest. In contrast, the reflective vs. dissipative processes of the inclined plane on the impacting bores and their spreading lengths has been highlighted when decreasing β. Particularly, the latter dissipative process induces a decrease of the first bore runup as well as a runup of the second one smaller than the first one bore-backwash collision. This extra-dissipation process leads to a minimal value of the second bore runup for a given Δt at small β. Yet, an enhancement of the second bore extension has been observed in bore-backwash collision regime at large β. When increasing β, backwash of the first bore is initiated before its entire water mass has been transferred to the swash, limiting the influence of its backwash on the following bore. This process depends on the ratio η_b/L (wave steepness) compared to β, and thus on the initial hydrodynamic conditions. Such a process can actually be observed in the results of two solitary waves impacting an inclined plane reported in Pujara et al. (2015). In our case, $\eta_b/L \sim 1.5°$, which is of the order of the smaller $\beta = 6°$ (green curves) and significantly smaller than the other slopes. A transition of the bore-backwash collision processes at large $\beta/(\eta_b/L)$ is thus experimentally observed. The ballistic models for the evolution of the shoreline developed in the paper do not accounted for this process. This aspect warrants dedicated future research. However, these models have demonstrated the capability of simple, easily extendable models to predict the dynamics of the shoreline and corresponding runups, highlighting and quantifying the aforementioned observations.

Relevance to field observations. Overall, the laboratory model examined in this study enables the reproduction of qualitative field observations and facilitates the development of simple theoretical models to rationalize these observations and measurements. However, to validate the proposed physical model, field data would be necessary. Unfortunately, obtaining such data requires dedicated measurements that are not readily available. Nevertheless, to demonstrate the potential of this approach to predict field observations reasonably, some field data (García-Medina et al., 2017; Bergsma et al., 2019; Stringari and Power, 2020) and experimental data obtained in a large wave flume facility (Alsina et al., 2018) have been extracted from the literature and reported in Fig. 11. Although these data were not specifically designed for the quantities relevant to the present analysis, information can be extracted from these papers to estimate the maximum runup obtained from bore–bore merging processes compared to isolated ones

(see Fig. 11(c); in all cases, size of the symbols exceeds uncertainties in extraction). For example, in García-Medina et al. (2017), shoreline evolution data from Agate Beach, Oregon (USA), for a beach slope of $\beta \approx 1°$ is provided in a spatiotemporal diagram in their Fig. 1. This allows for the extraction of a ratio between the maximum and minimum runup, which is reported as an estimate of X_2^+ in Fig. 11(c) (lightest grey square). In Bergsma et al. (2019), data obtained from a 2D LiDAR height profiler at Nha Trang (Vietnam) are available. Their Fig. 5 allows estimating the upper beach slope, approximately $\beta \approx 11°$, while their Fig. 9 enables the measurement of a run-up event associated with bore–bore merging for a relatively small time lag between two consecutive events, as well as a run-up associated with a single bore. Their ratio is reported in Fig. 11(c) (darkest grey square). Additionally, an estimation of the swash period relative to the period of the incoming bore can be obtained from their Fig. 9(b). Here, it is considered as a relevant measure to calculate $\Delta t_{sc}^+ - \Delta t_{sm}^+$, which is depicted in Fig. 11(c) (dark grey squares). Due to the uncertainty in this measurement, two time scales are utilized as the characteristic time scale $T_{\Delta t}$ for non-dimensionalization. These correspond to the peak period of the incoming wave at Nha Trang, approximately 11 s, and an estimation of $L/c_b \approx 7.6$ s derived from their data. In Stringari and Power (2020), data from seven Australian beaches are given, allowing for the extraction of $X_2^+(\beta)$ as the ratio between runups obtained for wave capture processes (bore–bore merging) and non-capture ones. These data are also reported in Fig. 11(c) (intermediate light grey squares). Furthermore, data from experiments performed in a large-scale wave flume in Alsina et al. (2018) provide estimations of the ratio between maximum runup associated with merging and single swash events for different beach states with upper beach slopes $\beta \approx 6.5°$ and $\beta \approx 11.5°$ (their Figs. 2, 5 and 9). These values are also reported in Fig. 11(c) (intermediate dark grey squares). By comparing these data from different studies, including field data, with the trend reported in Fig. 11, the potential of the proposed approach is promising. However, further dedicated data collection in future studies would be beneficial.

CRediT authorship contribution statement

José Barale: Writing – original draft, Methodology, Investigation, Formal analysis, Data curation, Conceptualization. **Laurent Lacaze:** Writing – review & editing, Writing – original draft, Validation, Supervision, Methodology, Investigation, Formal analysis, Data curation, Conceptualization. **Dominique Astruc:** Supervision, Methodology, Conceptualization. **Rafael Almar:** Conceptualization. **Luis Pedro Almeida:** Conceptualization.

Declaration of competing interest

The authors declare that they have no known competing financial interests or personal relationships that could have appeared to influence the work reported in this paper.

Data availability

Data will be made available on request.

Acknowledgements

This research was funded by the University of Toulouse UFTMIP, France (IDEX UNITI Program 'Transversalité' AAP 2015 – SWASH LAB). LL was also funded by a CNRS-80PRIME project.

The authors would like to thank Serge Font and Jean-Dominique Baron for technical support in designing and manufacturing the experimental device.

Appendix A. Catch-up process in the inner-surf : single wave model for the second bore

To highlight the catch-up process for $\Delta t < \Delta t_{cu}$, we propose to model the evolution of the second bore, based one a Stoker-type solution built upon the background evolution of the first bore as they both travel from the initial reservoirs towards the beach face.

First, at $t = \Delta t$, one assumes the second bore to be a Stoker-type solution, with an upstream condition of water height $h_{t1}(\Delta t) = h(x = -l_1, t = \Delta t)$ and velocity $u_{t1}(\Delta t) = u(x = -l_1, t = \Delta t)$. The latter upstream condition models the background flow induced by the tail of the first bore, subscript t, at the position of the second bore generation ($x = -l_1$). Note that this condition replaces the upstream condition of a water layer h_0 at rest used to describe the first bore in Section 3. In this context, at $t = \Delta t$, the second bore height $h_{b2}(\Delta t)$ is found to be a solution of

$$\left(\frac{u_{t1}(\Delta t)}{\sqrt{g h_1}} + 2\sqrt{\frac{h_{b2}(\Delta t)}{h_1}} - 2\right)^2 - \frac{1}{2}\frac{\left(h_{b2}(\Delta t) - h_{t1}(\Delta t)\right)^2}{h_1} \times \left(\frac{1}{h_{b2}(\Delta t)} + \frac{1}{h_{t1}(\Delta t)}\right) = 0. \tag{A.1}$$

Then, for $t > \Delta t$, the second bore is supposed to climb on the tail of the preceding one, as observed in Section 5.1. Flow conditions upstream the second bore thus evolve in time while the second bore climbs on the first one. In this context, one assumes that (i) the second bore height h_{b2} remains unchanged during its evolution, (ii) the second bore dynamics satisfy the hydraulic jump conditions at the bore position and (iii) the flow conditions imposed by the first bore on the second one are not affected by the presence of the second one. (i) reads $h_{b2}(t) = h_{b2}(\Delta t)$ with $h_{b2}(\Delta t)$ obtained from Eq. (A.1). (iii) means that the local flow conditions upstream the second bore, $h(x_{b2}^+(t), t) = h_{t1}(t)$ and $u(x_{b2}^+(t), t) = u_{t1}(t)$, can be extracted from the single bore situation. Then, applying conservation of mass flux and conservation of moment flux across the bore, (ii), the second front bore celerity can be written as

$$c_{b2}(t) = u_{t1}(t) + \sqrt{\frac{g}{2} h_{b2}(\Delta t)\left(\frac{h_{t1}(t) + h_{b2}(\Delta t)}{h_{t1}(t)}\right)}. \tag{A.2}$$

The background evolution induced by the first bore is obtained for $\Delta t = \infty$, i.e. for a single bore configuration when no second bore is generated. The spatio-temporal diagram of its water elevation $\eta(x, t)$ is shown in Fig. A.12 (colourmap of η in each frame, star symbols correspond to the position of the background bore). The local value of $h_{t1}(t)$ can typically be extracted from this diagram, while $u_{t1}(t)$ is estimated assuming a local conservation of max flux emanating from jump-type condition, $u_{t1}(t)h_{t1}(t) = c_{b1}(h_{t1}(t) - h_0)$. Using (A.1) and (A.2), the temporal evolution of the second bore position can be predicted (see Fig. A.12(a); blue full symbols, circles obtained for $\Delta t = 0.4$ s and squares for $\Delta t = 0.6$ s). Such prediction can be compared to the actual evolution of the second bore $x_{b2}(t)$ extracted from experimental data, also with $\Delta t = 0.4$ s (open black circles) and $\Delta t = 0.6$ s (open black squares). Clearly, a similar trend is obtained between experimental data and model prediction of the second bore, highlighting the bore acceleration reported as the catch-up process in Section 5.1. However, model slightly overestimates the acceleration of the second bore. Given the strong assumption on the condition upstream the second bore evolution $u_{t1}(t)$, the case for which $u_{t1}(t)$ is set to zero in Eq. (A.2) is also shown in Fig. A.12(b) (green full symbols, circles $\Delta t = 0.4$ s and squares $\Delta t = 0.6$ s). In this case, the acceleration is slightly underestimated. The condition $u_{t1}(t)$ has therefore a significant influence on the quantitative prediction of the bore evolution, while the qualitative behaviour is shown to be relevant using such modelling. Unfortunately, prediction of $u_{t1}(t)$ remains difficult. For sake of parameterization, one proposes here to replace $u_{t1}(t)$ following the previous estimation by $u_{t1}(t) = 0.5c_{b1}(h_{t1}(t) - h_0)/h_{t1}(t)$ in the model. Such solution is shown in

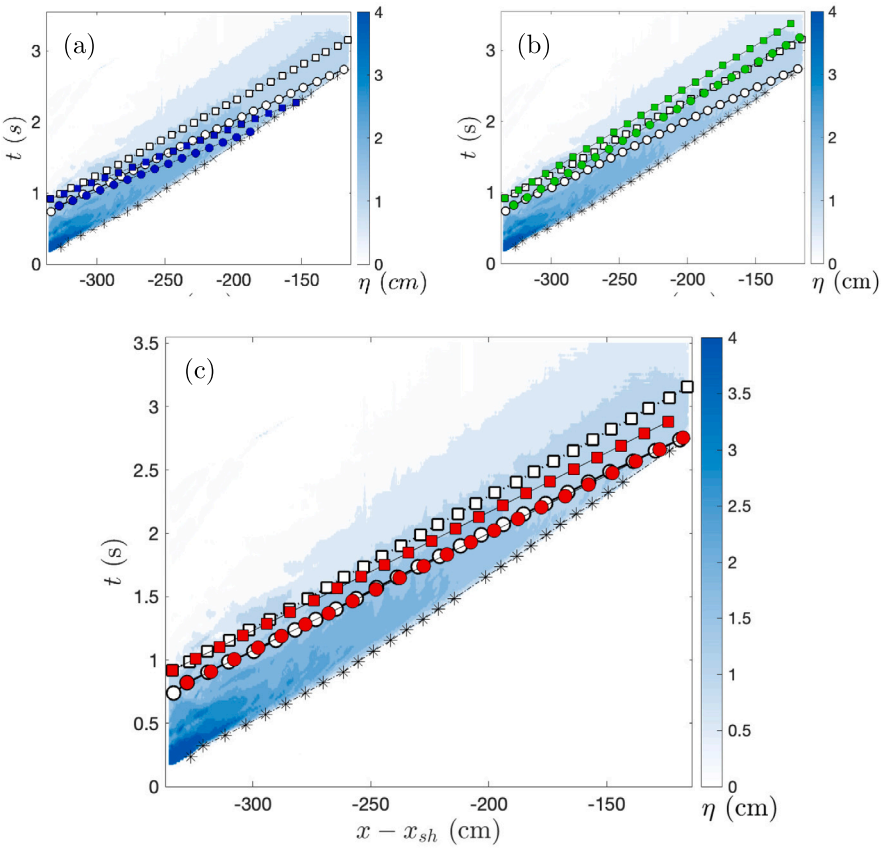

Fig. A.12. Evolution of the two successive bores. Comparison between experimental measurements (open symbols) and models (see text for details on frame (a), frame (b) and frame (c) respectively) (full symbols) for $\Delta t = 0.4$ s (circles) and $\Delta t = 0.6$ s (squares).

Fig. A.12(c) (red full symbols, circles $\Delta t = 0.4$ s and squares $\Delta t = 0.6$ s). The agreement between the model and the data has been significantly enhanced by incorporating the parametrization factor. Yet, the physical process leading to the coefficient 0.5 is not understood, it can be noted that the evolving wave is not a strictly steady structure in the frame moving with the bore. Then the initial model of mass conservation with a coefficient 1 shall failed to be satisfied. Given that the wave shape spreads slightly in the horizontal direction (see contours in Fig. A.12), this explains why a factor smaller than 1 is found to be a better parameterization of the model.

This approach allows to capture the catch-up process and can therefore be easily used to predict front bore dynamics in the inner-surf. This will serve as the primary mechanism for proposing a model of the evolution of two successive bores in the inner-surf in Section 5.2.

Appendix B. Ballistic model and initial condition for the swash induced by the second bore

Models *A* and *B* depict the dynamics of the swash front caused by the second bore, building upon a ballistic equation akin to the one employed for the initial swash event (5). In both cases, the depth of the initial swash is disregarded when solving the system for the subsequent swash. Thus, the swash geometry mirrors that of the preceding bore (refer to Fig. 9(a)). The influence of the first swash on the second one is then incorporated either through the initial condition for the first bore (model *A*) or via the bottom boundary condition (model *B*).

Model A. In this model, Eq. (5) is solved for the second swash using the following initial condition at $(t = t_{s2}, X = 0)$, i.e. when the second bore reaches the shoreline at rest

$$\frac{dX_{s2}}{dt} = 2\sqrt{g\eta_b \cos\beta} + 0.5\frac{dX_{s1}}{dt} \quad \text{if} \quad t_{s2} < T_{s1}, \tag{B.1}$$

$$\frac{dX_{s2}}{dt} = 2\sqrt{g\eta_b \cos\beta} \quad \text{if} \quad t_{s2} > T_{s1}, \tag{B.2}$$

with T_{s1} representing the time at which the swash induced by the first bore ends, i.e. $X_{s1}(T_{s1}) = 0$. For $t_{s2} > T_{s1}$, the second bore is subjected to the same condition as the first one, resulting in no interaction between the two bores. Note that, T_{s1} depends on both β and t_{s1} and includes the initial lag Δt. Such model implies that the dynamics of the first swash during the second swash is not considered, as it solely affects its initial condition. However, the influence of the first bore on the dynamics of the second bore is incorporated through dX_{s1}/dt at $t = t_{s2}$ in (B.2), which can be derived from (5) and can either be positive, resulting in bore-runup merging, or negative, leading to bore-backwash collision. The coefficient 0.5 in (B.2) has been adjusted using experimental data $(\beta = 11°, \Delta t = \Delta_{sm})$. Note that this value is somewhat similar to the coefficient obtained in Appendix A when incorporating the tail velocity of the preceding bore as an additional term in the dynamics of the second bore.

Model B. This model considers the interaction between the two swash events, on finite time, while maintaining the same initial velocity condition for both bores. Here, it is assumed that the friction term at

the bottom is altered by the presence of the first swash until the second swash reaches the first one, i.e. at $X_{s2} = X_{s1} = X_i$. Simultaneously, the weight term along the slope for the second swash is neglected when $dX_{s1}/dt > 0$, indicating saturation during the run-up of the first swash. Consequently, the ballistic model Eq. (5) is modified as:

$$\begin{aligned}
\frac{d^2X_{s2}}{dt^2} &= -\frac{C_D^{eff}}{h_s(t)}\left(\frac{dX_{s2}}{dt} - \frac{dX_{s1}}{dt}\right)\left|\frac{dX_{s2}}{dt} - \frac{dX_{s1}}{dt}\right| \\
&\qquad \text{if} \quad (dX_{s1}/dt > 0, X_{s2} < X_{s1}), \\
\frac{d^2X_{s2}}{dt^2} &= -g\sin\beta - \frac{C_D^{eff}}{h_s(t)}\left(\frac{dX_{s2}}{dt} - \frac{dX_{s1}}{dt}\right)\left|\frac{dX_{s2}}{dt} - \frac{dX_{s1}}{dt}\right| \\
&\qquad \text{if} \quad (dX_{s1}/dt < 0, X_{s2} < X_{s1}), \\
\frac{d^2X_{s2}}{dt^2} &= -g\sin\beta - \frac{C_D^{eff}}{h_s(t)}\left(\frac{dX_{s2}}{dt}\right)\left|\frac{dX_{s2}}{dt}\right| \quad \text{otherwise},
\end{aligned} \tag{B.3}$$

with $(X_{s2} = 0, dX_{s2}/dt = 2\sqrt{g\eta_b\cos\beta})$ at $t = t_{s2}$.

References

Alsina, J.M., Cáceres, I., 2011. Sediment suspension events in the inner surf and swash zone. measurements in large-scale and high-energy wave conditions. Coast. Eng. 58, 657–670.

Alsina, J.M., Zanden, J.Van.der., Caceres, I., Ribberink, J.S., 2018. The influence of wave groups and wave-swash interactions on sediment transport and bed evolution in the swash zone. Coast. Eng. 140, 23–42.

Antuono, M., Hogg, A.J., 2009. Run-up and backwash bore formation from dam-break flow on an inclined plane. J. Fluid Mech. 640, 151–164.

Astruc, D., Cazin, S., Cid, E., Eiff, O., Lacaze, L., Robin, P., Toublanc, F., Cáceres, I., 2012. A stereoscopic method for rapid monitoring of the spatio-temporal evolution of the sand-bed elevation in the swash zone. Coast. Eng. 60, 11–20.

Baldock, T., Alsina, J., Caceres, I., Vicinanza, D., Contestabile, P., Power, H., Sanchez-Arcilla, A., 2011. Large-scale experiments on beach profile evolution and surf and swash zone sediment transport induced by long waves, wave groups and random waves. Coast. Eng. 58, 214–227.

Baldock, T., Holmes, P., 1999. Simulation and prediction of swash oscillations on a steep beach. Coast. Eng. 36, 219–242.

Bergsma, E.W., Blenkinsopp, C.E., Martins, K., Almar, R., de Almeida, L.P.M., 2019. Bore collapse and wave run-up on a sandy beach. Cont. Shelf Res. 174, 132–139.

Bertin, X., Bakker, A.de., Dongeren, A.Van., Coco, G., André, G., Ardhuin, F., Bonneton, P., Bouchette, F., Castelle, B., Crawford, W.C., et al., 2018. Infragravity waves: From driving mechanisms to impacts. Earth-Sci. Rev. 177, 774–799.

Brocchini, M., Baldock, T.E., 2008. Recent advances in modeling swash zone dynamics: Influence of surf-swash interaction on nearshore hydrodynamics and morphodynamics. Rev. Geophys. 46.

Cáceres, I., Alsina, J.M., 2012. A detailed, event-by-event analysis of suspended sediment concentration in the swash zone. Cont. Shelf Res. 41, 61–76.

Chen, B.T., Kikkert, G.A., Pokrajac, D., Dai, H.J., 2016. Experimental study of bore-driven swash–swash interactions on an impermeable rough slope. Coast. Eng. 108, 10–24.

Chen, W., Van Der Werf, J.J., Hulscher, S.J.M.H., 2023. A review of practical models of sand transport in the swash zone. Earth-Sci. Rev. 238, 104355.

da Silva, P.G., Coco, G., Garnier, R., Klein, A.H.F., 2020. On the prediction of runup, setup and swash on beaches. Earth-Sci. Rev. 204, 103148.

De Bakker, A., Tissier, M., Ruessink, B., 2016. Beach steepness effects on nonlinear infragravity-wave interactions: A numerical study. J. Geophys. Res.: Oceans 121, 554–570.

Erikson, L., Larson, M., Hanson, H., 2005. Prediction of swash motion and run-up including the effects of swash interaction. Coast. Eng. 52, 285–302.

García-Medina, G., Özkan-Haller, H.T., Holman, R.A., Ruggiero, P., 2017. Large runup controls on a gently sloping dissipative beach. J. Geophys. Res.: Oceans 122, 5998–6010.

Guard, P.A., Baldock, T.E., 2007. The influence of seaward boundary conditions on swash zone hydrodynamics. Coast. Eng. 54, 321–331.

Hibberd, S., Peregrine, D., 1979. Surf and run-up on a beach: A uniform bore. J. Fluid Mech. 95, 323–345.

Hogg, A.J., 2006. Lock-release gravity currents and dam-break flows. J. Fluid Mech. 569, 61–87.

Hughes, M.G., Baldock, T.E., Aagaard, T., 2018. Swash saturation: An assessment of available models. Ocean Dyn. 68, 911–922.

Hughes, M.G., Moseley, A.S., 2007. Hydrokinematic regions within the swash zone. Cont. Shelf Res. 27, 2000–2013.

Lo, Hong-Yueh, Park, Yong Sung, Liu, Philip L-F, 2013. On the run-up and back-wash processes of single and double solitary waves—An experimental study. Coastal engineering 80, 1–14.

Mory, M., Abadie, S., Mauriet, S., Lubin, P., 2011. Run-up flow of a collapsing bore over a beach. Eur. J. Mech. B Fluids 30, 565–576.

Padilla, E.M., Alsina, J.M., 2017. Transfer and dissipation of energy during wave group propagation on a gentle beach slope. J. Geophys. Res.: Oceans 122, 6773–6794.

Pedersen, G.K., Lindstrøm, E., Bertelsen, A.F., Jensen, A., Laskovski, D., Sælevik, G., 2013. Runup and boundary layers on sloping beaches. Phys. Fluids 25, 012102.

Pujara, N., Liu, P.L.F., Yeh, H.H., 2015. An experimental study of the interaction of two successive solitary waves in the swash: A strongly interacting case and a weakly interacting case. Coast. Eng. 105, 66–74.

Rottman, J.W., Simpson, J.E., 1983. Gravity currents produced by instantaneous releases of a heavy fluid in a rectangular channel. J. Fluid Mech. 135, 95–110.

Rutten, J., Torres-Freyermuth, A., Puleo, J.A., 2021. Uncertainty in runup predictions on natural beaches using xbeach nonhydrostatic. Coast. Eng. 166, 103869.

Shen, M.C., Meyer, R.E., 1963. Climb of a bore on a beach part 3. run-up. J. Fluid Mech. 16, 113–125.

Stansby, P., Chegini, A., Barnes, T., 1998. The initial stages of dam-break flow. J. Fluid Mech. 374, 407–424.

Stockdon, H.F., Holman, R.A., Howd, P.A., Sallenger, Jr., A.H., 2006. Empirical parameterization of setup, swash, and runup. Coast. Eng. 53, 573–588.

Stoker, J.J., 1957. Waler waves: The mathematical theory with applications. Intersciences.

Streicher, M., Kortenhaus, A., Marinov, K., Hirt, M., Hughes, S., Hofland, B., Scheres, B., Schüttrumpf, H., 2019. Classification of bore patterns induced by storm waves overtopping a dike crest and their impact types on dike mounted vertical walls–A large-scale model study. Coast. Eng. J. 61, 321–339.

Stringari, C.E., Power, H.E., 2020. Quantifying bore-bore capture on natural beaches. J. Geophys. Res.: Oceans 125, e2019JC015689.

Tissier, M., Bonneton, P., Michallet, H., Ruessink, B.G., 2015. Infragravity-wave modulation of short-wave celerity in the surf zone. J. Geophys. Res.: Oceans 120, 6799–6814.

Yeh, H.H., Ghazali, A., Marton, I., 1989. Experimental study of bore run-up. J. Fluid Mech. 206, 563–578.

Zhang, Q., Liu, P.L.F., 2008. A numerical study of swash flows generated by bores. Coast. Eng. 55, 1113–1134.

Zhu, F., Dodd, N., 2015. The morphodynamics of a swash event on an erodible beach. J. Fluid Mech. 762, 110–140.